Database of Friction Angles of Sand and Consolidation Characteristics of Sand, Silt, and Clay

Knut H. Andersen, M.ASCE[1]; and Knut Schjetne[2]

Abstract: The paper presents diagrams of the (1) drained and undrained effective stress friction angles of sand; (2) dilatancy angle of sand; (3) parameters in a nonlinear constrained modulus expression for virgin loading, unloading, and reloading on sand and silt; and (4) diagrams with the coefficient of permeability for sand, silt, and clay. The database parameters are suitable for preliminary assessments or applications when assumed parameters are acceptable. The database can also be helpful in planning and interpreting site-specific tests and in reducing the number of site-specific tests. For important projects the parameters should be determined by site-specific tests. **DOI: 10.1061/(ASCE)GT.1943-5606.0000839.** © *2013 American Society of Civil Engineers.*

CE Database subject headings: Databases; Friction; Dilatancy; Soil permeability; Silts; Clays; Sand (soil type); Soil consolidation.

Author keywords: Database; Friction angle; Dilatancy angle; Constrained modulus; Permeability.

Introduction

Friction angles and consolidation characteristics are important parameters in many geotechnical analyses performed both on land and offshore. Capacity analyses for drained loading require the drained peak friction angles, and the constant volume friction angles and dilatancy angles can also be relevant. The undrained effective stress friction angle is needed for effective stress analyses of undrained conditions, such as in the design of structures under cyclic loading from waves or wind.

Settlement calculations require the modulus for virgin loading, reloading, or unloading conditions, depending on the actual load history of the soil deposit and the foundation. The constrained soil modulus is nonlinear, and it also depends on the stress history; i.e., virgin loading versus unloading and reloading. For instance, dissipation of cyclically induced pore pressure is a reloading situation and requires the reloading modulus. The various moduli may also be needed in cases with pore-pressure redistribution within the soil. The use of constrained modulus assumes one-dimensional (1D) conditions. This is a realistic assumption for the soil beneath structures where the diameter of the structure is large compared with the depth of influence in the soil, and can also be a reasonable approximation in many other situations. For important projects, the various soil parameters should be determined by site-specific tests; however, in preliminary assessments or applications when assumed parameters are acceptable, databases can provide valuable guidance. Databases can also be helpful in planning and interpreting site-specific tests and in reducing the number of site-specific tests.

[1]Technical Director, Norwegian Geotechnical Institute, P.O. Box 3930, Ullevaal Stadion, N-0806 Oslo, Norway (corresponding author). E-mail: kha@ngi.no

[2]Senior Engineer, Norwegian Geotechnical Institute, P.O. Box 3930, Ullevaal Stadion, N-0806 Oslo, Norway.

Note. This manuscript was submitted on July 7, 2011; approved on September 17, 2012; published online on September 19, 2012. Discussion period open until December 1, 2013; separate discussions must be submitted for individual papers. This paper is part of the ***Journal of Geotechnical and Geoenvironmental Engineering***, Vol. 139, No. 7, July 1, 2013. ©ASCE, ISSN 1090-0241/2013/7-1140–1155/$25.00.

This paper presents a database of the (1) drained and undrained effective stress friction angles; (2) dilatancy angle; (3) virgin, unloading, and reloading constrained moduli; and (4) coefficient of permeability. The friction and dilatancy angles are mostly for sand with little or no silt content. The constrained moduli are on sand and silt. The permeability covers sand, silt, and clay. The data are compiled from the Norwegian Geotechnical Institute (NGI) files and published literature. The databases of other parameters, such as the undrained shear strength, strength anisotropy, rate effect, initial shear modulus, reconsolidated remolded strength, and thixotropy of clay, can be found in Bjerrum (1973), Ladd et al. (1977), Lunne and Andersen (2007), and Andersen et al. (2008). The parameters for the cyclic shear strength of clay, sand, and silt are presented in Andersen (2009).

Friction Angles

The friction angle database consists of more than 500 triaxial compression tests on 54 different sands from 38 different sites. Approximately 40–50% of the tests are from offshore sites. The remaining sites show a wide geographical scatter and include beach sands, river sands, and sands from onshore sites. Eighty percent of the sands contain no silt (particles < 0.06 mm). The highest silt content is 13% in one sample. The mean particle size of the sands, D_{50}, is 0.23 mm, whereas the average coefficient of uniformity is $C_u = D_{60}/D_{10} = 1.95$. The quartz content of the sands is on average 85% with a SD of 17%. For 75% of the sands, the grain shape has been reported, and varies from rounded to angular. The most typical characterization is subangular. Calcareous soils are not included. The experience from the data available at NGI is that calcareous soils have higher friction angles than noncalcareous soils, at least at low consolidation stresses.

General Principles and Definitions

Fig. 1 shows the typical results from triaxial tests on dense and loose sands sheared in compression in terms of the stress-strain curves and stress paths. The drained tests on dense sand show a peak on the stress-strain curve and a peak friction angle ϕ'_p, followed by a continuous decrease in shear stress to large strains in which the

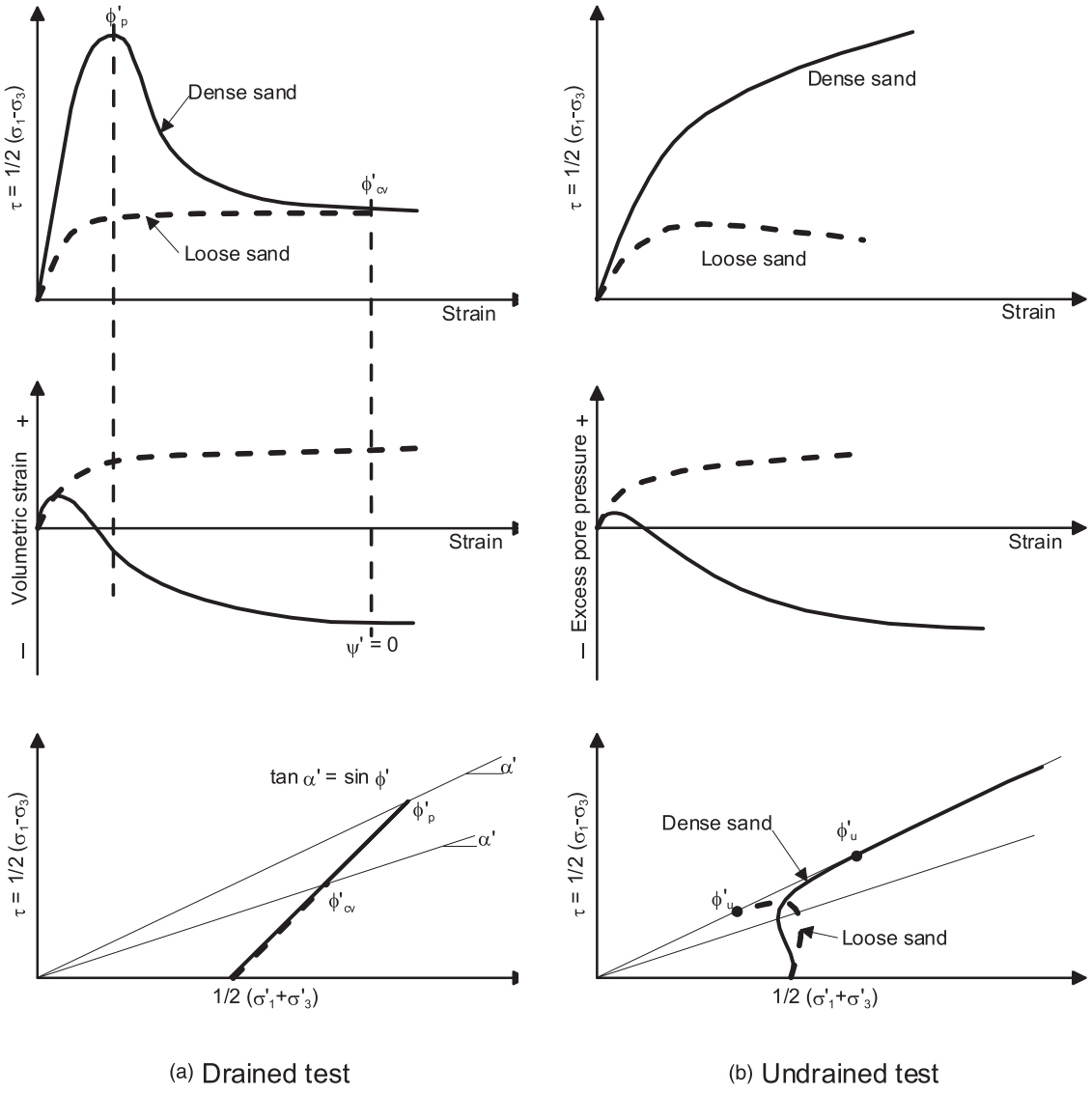

Fig. 1. Definition of friction angles in tests on loose and dense sands: (a) drained test; (b) undrained test

friction angle value may reduce to an ultimate value, ϕ'_{cv}, where cv denotes constant volume. As seen from Fig. 1(a), the dense sand initially contracts and then expands (dilates) strongly until the end of the test. The drained tests on loose sand showed no peak shear stress but rather a stress-strain curve that flattened out at large strains after substantial compression. Loose specimens also reached an ultimate state with constant shear stress, increasing shear strain and zero volumetric strain defined by a constant volume friction angle, ϕ'_{cv}.

The undrained tests on dense sand showed a shear stress that kept increasing to large strains, as illustrated in Fig. 1(b). The undrained tests included pore-water pressure measurements, which showed that the pore-water pressure may increase at small strains but decrease with increasing strains. The effective stress path followed close to the failure line defined by the undrained effective stress friction angle, ϕ'_u. The undrained tests on loose sand may show a peak shear stress at a moderate strain and an increase in pore-water pressure and a decrease in shear stress with increasing shear strain. At large strains the stress path followed a failure line defined by ϕ'_u. There was a connection between the shear strain–induced volumetric strain in drained tests and the excess pore-water pressure in undrained tests. Loose specimens contracted in the drained tests and generated positive pore pressure in the undrained tests. Dense specimens expanded in the drained tests and generate negative pore pressure in the undrained tests.

The friction angles ϕ'_p, ϕ'_{cv}, and ϕ'_u are presented subsequently, where they are related to the relative density and effective octahedral consolidation stress, ϕ_c'. All friction angles are defined by the secant values and zero cohesion intercept. The number of tests and the typical compositional properties are included in the various correlation charts in Figs. 2, 4, 5, 7 and 9 in terms of the number of tests (n), mean value (μ), and SD (σ). The curves in the diagrams represent the calculated mean values for various σ'_c intervals. There is considerable scatter in the data; however, the trends are still clear. Some curves may overlap because of scatter in the results and limited number of data. No attempt has been made to avoid this overlap.

The determination of e_{min} and e_{max} in calculating the relative density, D_r, is seldom specified. However, for most of the tests carried out at NGI, e_{min} is determined by a special NGI procedure in which the specimen is built into a mold in six layers, and each layer is vibrated by a pneumatic hammer that applies vibrations directly on to the specimen. This gives a somewhat lower e_{min} than, for example,

J. Geotech. Geoenviron. Eng., 2013, 139(7): 1140-1155

the procedure according to BS 1377, Part 4, Clause 4 [British Standards Institute (BSI) 1990].

Drained Peak Friction Angle

The drained peak friction angle, ϕ_p', from all the tests is plotted in Fig. 2, which shows that ϕ_p' increases with increasing relative density D_r and decreases with increasing effective consolidation stress level ϕ_c'. For very high consolidation stresses above 5,000 kPa, the high stresses suppress the tendency to dilate, and ϕ_p' seems constant and independent of D_r. At these high consolidation stresses this is also likely caused by particle crushing, even for quartz grains.

The data showed a tendency for ϕ_p' to increase with decreasing quartz content. This is somewhat surprising because quartz grains are supposedly harder than the other minerals that dominate sand, such as feldspars, mica, and calcite. However, an increased friction angle with increasing content of feldspar was confirmed by Bolton (1986). Angular particles seemed to give a higher ϕ_p' than the well-rounded ones; however, the effect was not clear. There was a slight trend for ϕ_p' to increase with increasing mean particle size, D_{50}. No obvious correlation was found between ϕ_p' and the coefficient of uniformity. These relationships have not been presented in the present paper because of space limitations.

The peak angle of internal friction versus relative density has been compared with available data in the literature. Bolton (1986) presented a correlation of the maximum angle of internal friction, ϕ'_{max}, to the friction angle of very loose sand with zero dilation, ϕ'_{crit}. For quartz, $\phi'_{crit} = 33°$ is suggested, and the resulting ϕ'_{max} from triaxial tests can be computed as $\phi_p' = \phi'_{crit} + 3I_R$, where $I_R = D_r(10 - \ln p') - 1$. In Fig. 3, two sets of ϕ_p' computed in this way have been presented for $p' = 150$ and 600 kPa; i.e., the stress range suggested by Bolton (1986). Here, p' is the average stress at failure, and for drained compression tests with a friction angle between 35 and 40° the corresponding average consolidation stress, ϕ_c', is of the order of 60% of the stress at failure. These curves correlate very well with the relevant empirical curves from the NGI database.

Two curves from Schmertmann (1978) are also included in Fig. 3 for uniform fine sand and uniform medium sand. These curves compare favorably with the empirical curves from the NGI database. Schmertmann (1978) suggested that the peak friction angle increases with the grain size of the sand; however, this is not supported by the NGI database.

Drained Constant Volume Friction Angle

The constant volume friction angles, ϕ'_{cv}, from all the tests are plotted in Fig. 4, which shows that ϕ'_{cv} increases with increasing relative

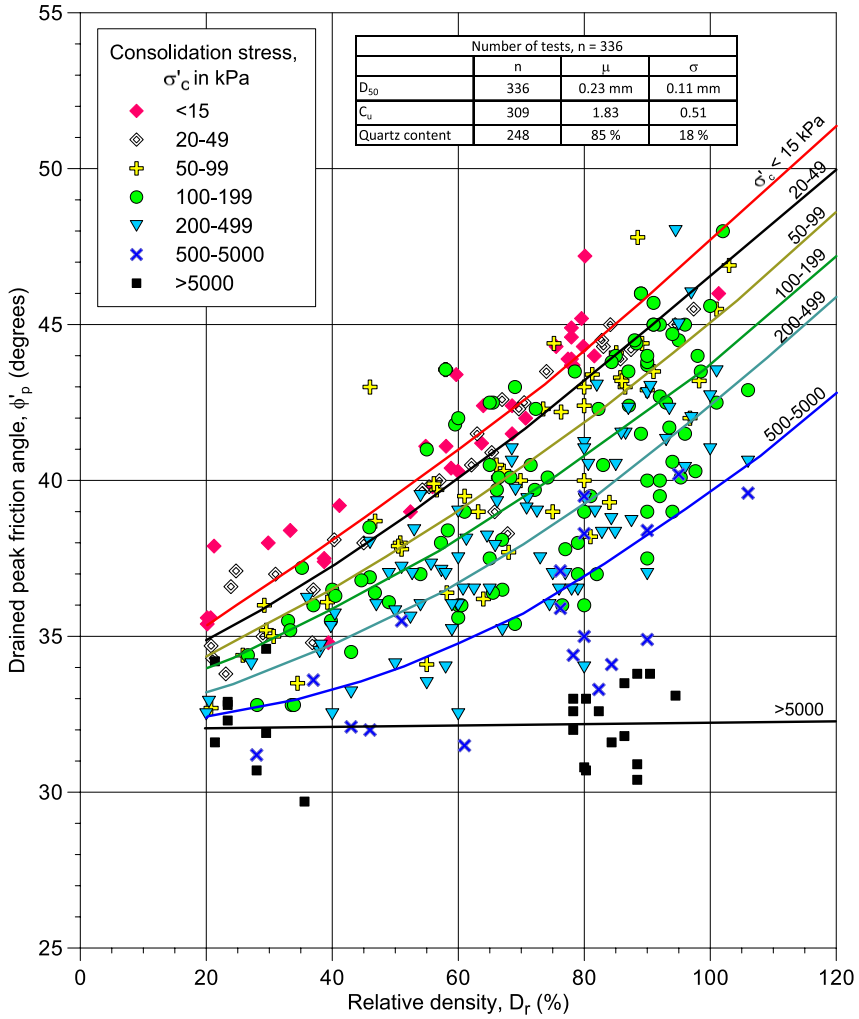

Fig. 2. (Color) Drained peak friction angle, ϕ_p', as a function of D_r and σ_c'

J. Geotech. Geoenviron. Eng., 2013, 139(7): 1140-1155

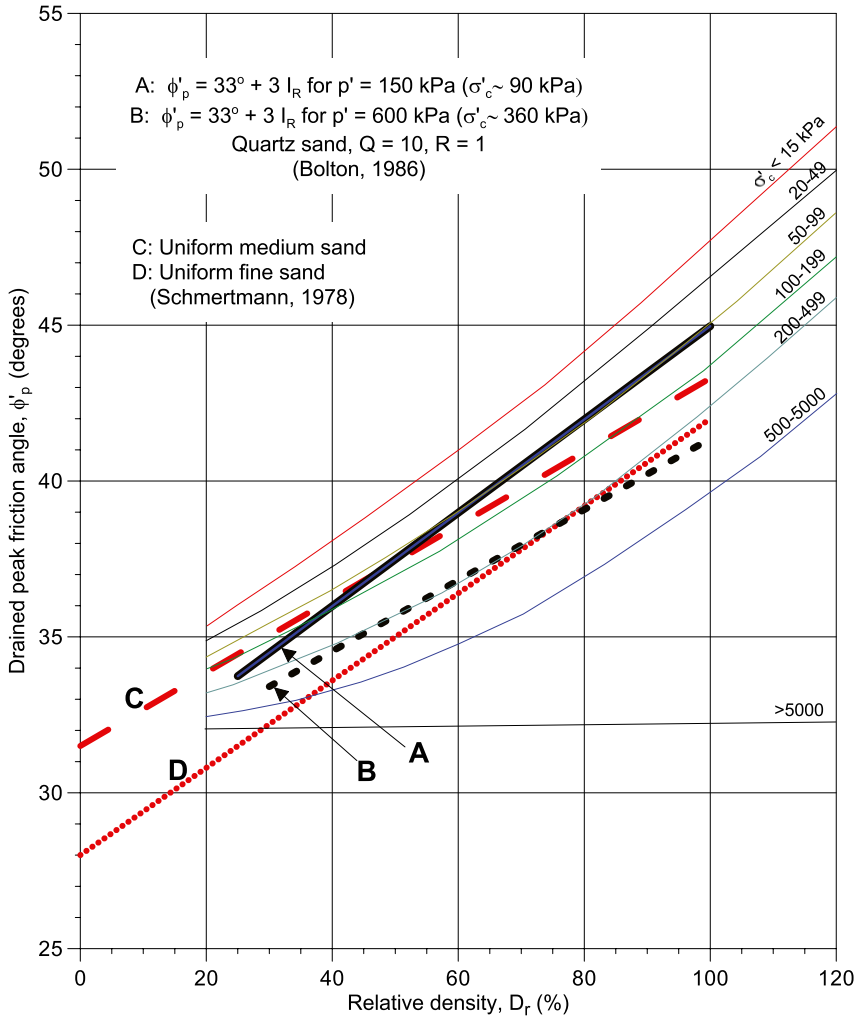

Fig. 3. Drained peak friction angle, ϕ'_p, compared with data from Schmertmann (1978) and Bolton (1986)

density, D_r, and decreasing effective consolidation stress, σ'_c. The data showed no effect of quartz content or angularity.

Undrained Effective Stress Friction Angle

The undrained effective stress friction angle, ϕ'_u, increases with increasing shear strain. In Fig. 5, ϕ'_u is plotted for a shear strain of 6%. Ideally, it would be best to use the shear strain where the failure envelope in the effective stress path plot approaches a straight line. Most tests were not run much further than 6% shear strain, particularly tests on dense sand that dilate, and were terminated because of practical limitations. The number of data points was significantly reduced when a higher strain criterion was chosen. However, the measured increase in ϕ'_u from 6 to 15% shear strain was, on average, less than 1°. The data show that ϕ'_u increases with increasing D_r. For $\sigma'_c \geq 100$ kPa, there was no clear effect of consolidation stress.

Comparison of Drained and Undrained Friction Angles

The drained peak, drained constant volume, and undrained effective stress friction angles are compared in Fig. 6 for a consolidation stress range of $\sigma'_c = 250 - 500$ kPa. The comparison shows that ϕ'_p is significantly higher than ϕ'_{cv} and ϕ'_u at high relative density. The difference is less at lower D_r.

Dilatancy Angle ψ

The dilatancy angle was determined for 127 drained triaxial compression tests. The dilatancy angle in the triaxial test is defined as

$$\sin\psi = \frac{-d\varepsilon_{\text{vol}}}{2d\varepsilon_a - d\varepsilon_{\text{vol}}}$$

where $d\varepsilon_{\text{vol}}$ and $d\varepsilon_a$ = volumetric and axial strain increments, respectively. This definition of the dilatancy angle is the most commonly referred to in the literature (e.g., Bolton 1986). The tangent dilatancy angle at peak shear stress is shown in Fig. 7. The dilation is normally at its maximum at peak shear stress. Fig. 7 shows that ψ increases with increasing D_r and that it is relatively independent of σ'_c. The maximum angle of dilatancy, $\psi_{\max}$, versus relative density has been compared with available data in the literature. Bolton (1986) suggested that $(-d\varepsilon_{\text{vol}}/d\varepsilon_a)_{\max} = 0.3I_R$, where $I_R = D_r(10 - \ln p') - 1$. This implies that $\sin\psi_{\max} = 0.3I_R/(2 + 0.3I_R)$. In Fig. 8, two sets of $\psi_{\max}$ computed in this way have been presented for $p' = 150$ and 600 kPa; i.e., the stress range suggested by Bolton (1986). These curves show slightly higher dilatancy angles than the empirical curves from the NGI database, especially for high relative densities. The secant dilation angle was also determined at axial strain levels of $\varepsilon_a = 1$, 2.5, and 5%, and at peak shear stress for

J. Geotech. Geoenviron. Eng., 2013, 139(7): 1140-1155

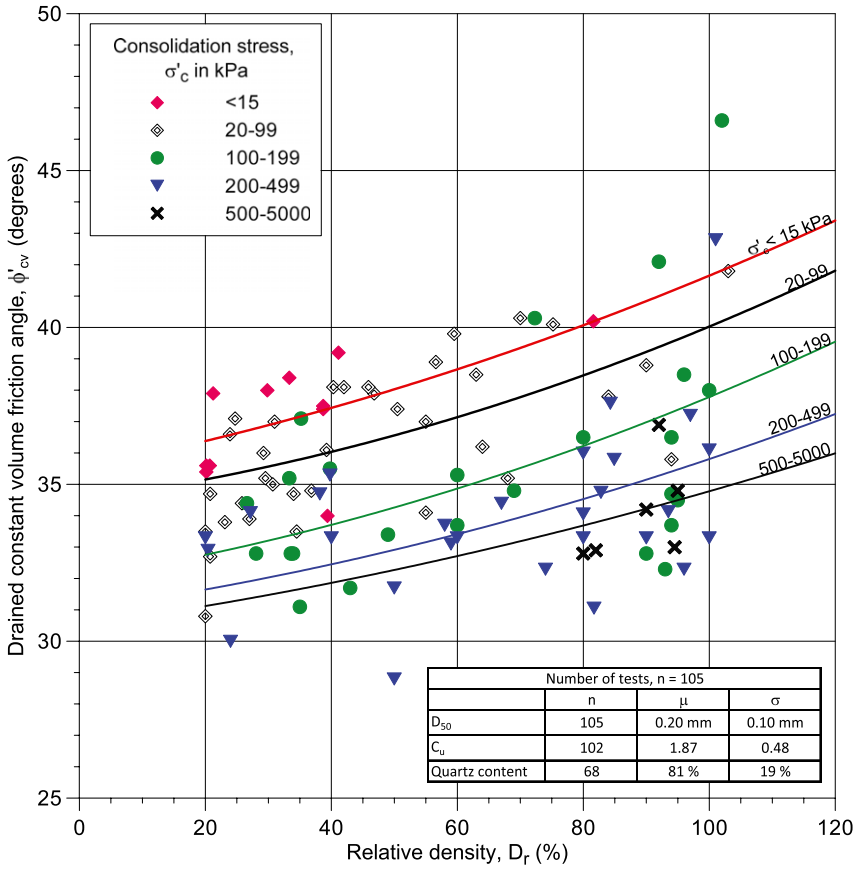

Fig. 4. (Color) Drained constant volume friction angle, ϕ'_{cv}, as a function of D_r and σ'_c

some of the tests (Fig. 9). The stress range for these tests was $\sigma'_c = 150 - 450$ kPa. The secant dilation angle was corrected by subtracting the volumetric strain caused by the increase in normal stresses.

Constrained Modulus

Constrained Modulus Formulation

The constrained modulus is herein expressed by a nonlinear modulus formulation. An attempt is made to establish correlations between the parameters in this formulation and index parameters such as the water content, void ratio, and grain size parameters for sand and silt. The constrained modulus, M, is expressed as

$$M_l = m_l \cdot p_a \cdot \left(\sigma'_v/p_a\right)^{n_l}$$

$$M_u = m_l \cdot p_a \cdot \left(\sigma'_{v,\max}/p_a\right)^{n_l} \cdot\ m_u \cdot \left(\sigma'_v/\sigma'_{v,\max}\right)^{n_u}$$

$$M_r = m_l \cdot p_a \cdot \left(\sigma'_{v,\max}/p_a\right)^{n_l} \cdot\ m_r \cdot \left(\sigma'_v/\sigma'_{v,\max}\right)^{n_r}$$

where M_l, M_u, and M_r = tangential effective stress–normalized constrained modulus for the first loading (virgin), unloading, and reloading, respectively; m_l, m_u, and m_r = constrained modulus number for the first loading (virgin), unloading, and reloading, respectively; n_l, n_u, and n_r = constrained modulus exponent for the first loading (virgin), unloading, and reloading, respectively; p_a = atmospheric pressure (100 kPa); σ'_v = vertical effective stress; and $\sigma'_{v,\max}$ = maximum vertical effective stress prior to unloading.

The formulas distinguish between first loading, unloading, and reloading, and they model the higher moduli that normally occur during unloading and reloading compared with first loading. They also model nonlinear behavior both for first loading, unloading and reloading. The formulation for the first loading is similar to the one used, for instance, by Janbu (1963) and Hardin and Drnevich (1972); however, they used a first loading modulus exponent $n_l = 0.5$. In the study reported herein, the best-fit exponents for the available data were sought.

Assuming 1D conditions, the settlement of a structure can be calculated by integrating the vertical strains in the subsoil. The vertical strain, ε_v, which is valid for 1D conditions with no lateral strain, derived by integration of the proposed modulus expressions are as follows:

- Virgin loading from $\sigma'_{v,0}$ to σ'_v:

$$\varepsilon_v = \left[\left(\sigma'_v/p_a\right)^{1-n_l} - \left(\sigma'_{v,0}/\mathrm{p_a}\right)^{1-n_l}\right] \Big/ \left[m_l \cdot (1-n_l)\right] \cdot 100(\%)$$

- Unloading from $\sigma'_{v,\max}$ to σ'_v:

$$\varepsilon_v = \sigma'_{v,\max} \cdot \left[\left(\sigma'_v/\sigma'_{v,\max}\right)^{1-n_u} - 1\right] \Big/ \left\{p_a \cdot m_l \cdot \left(\sigma'_{v,\max}/p_a\right)^{n_l} \cdot \left[m_u \cdot (1-n_u)\right]\right\} \cdot 100(\%)$$

J. Geotech. Geoenviron. Eng., 2013, 139(7): 1140-1155

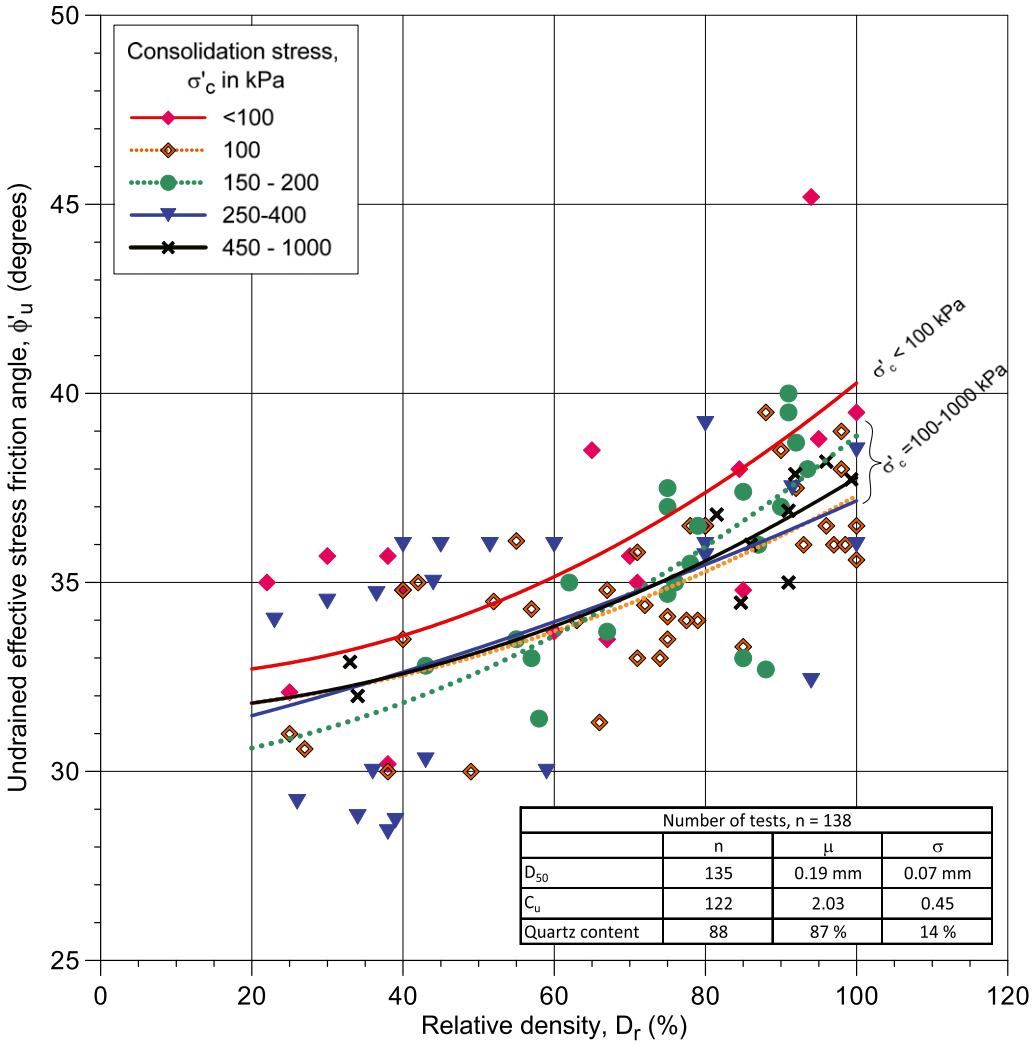

Fig. 5. (Color) Undrained effective stress friction angle, ϕ'_u, at 6% shear strain as a function of D_r and σ'_c

- Reloading from $\sigma'_{v,\min}$ to σ'_v:

$$\varepsilon_v = \sigma'_{v,\max} \cdot \left[\left(\sigma'_v/\sigma'_{v,\max}\right)^{1-n_r} - \left(\sigma'_{v,\min}/\sigma'_{v,\max}\right)^{1-n_r} \right] \Big/ \left\{ p_a \cdot m_l \cdot \left(\sigma'_{v,\max}/p_a\right)^{n_l} \cdot [m_r \cdot (1-n_r)] \right\} \cdot 100(\%)$$

Oedometer Tests

The oedometer test database consists of 49 oedometer tests; mainly on silt and sand with varying grain size, density, mineralogy, and angularity. Thirty-six of these were on noncalcareous soil. The interpretation is meant to focus on silt and sand; however, some tests with relatively high clay content were included because they may help establish trends for the parameter variations. The tests were run in a conventional oedometer with at least one unloading sequence. Most tests had two unload/reload sequences at various stress levels. Most of the tests with unloading had an overnight rest period before start of unloading. The results of the oedometer tests were influenced by false deformations of the oedometer system and by friction between the specimen and the oedometer ring. The measured vertical deformation was corrected for the false deformations based on deformations measured on a steel dummy. The oedometer ring was made as smooth as possible on the inside to minimize friction. No correction was made for side friction. Even if care is taken to reduce the effects of false deformation and inside friction, these factors may influence the results, especially the high unloading and reloading moduli for dense sand.

Best-Fit Parameters

Examples of the measured oedometer test data are presented in Fig. 10, which include the results of curve fitting with the proposed constrained modulus formulation. The curve fitting was done by calculating the vertical strain-log σ' curve by the previous equations and modifying the exponents to obtain the best fit. The best fit was based on visual judgment. The test was run with a constant rate of strain and had an overnight rest period of 16 h before start of unloading. It can be seen that significant creep occurred during the rest periods even if the sample had no clay content. The fines content was 60%. The rest period is not directly modeled in the curve fitting. In the modeling, the unload/reload curve is shifted to the start of the rest period. It is assumed that the creep will cause an apparent preconsolidation effect and that the loading curve will join the virgin loading curve at a stress above the

J. Geotech. Geoenviron. Eng., 2013, 139(7): 1140-1155

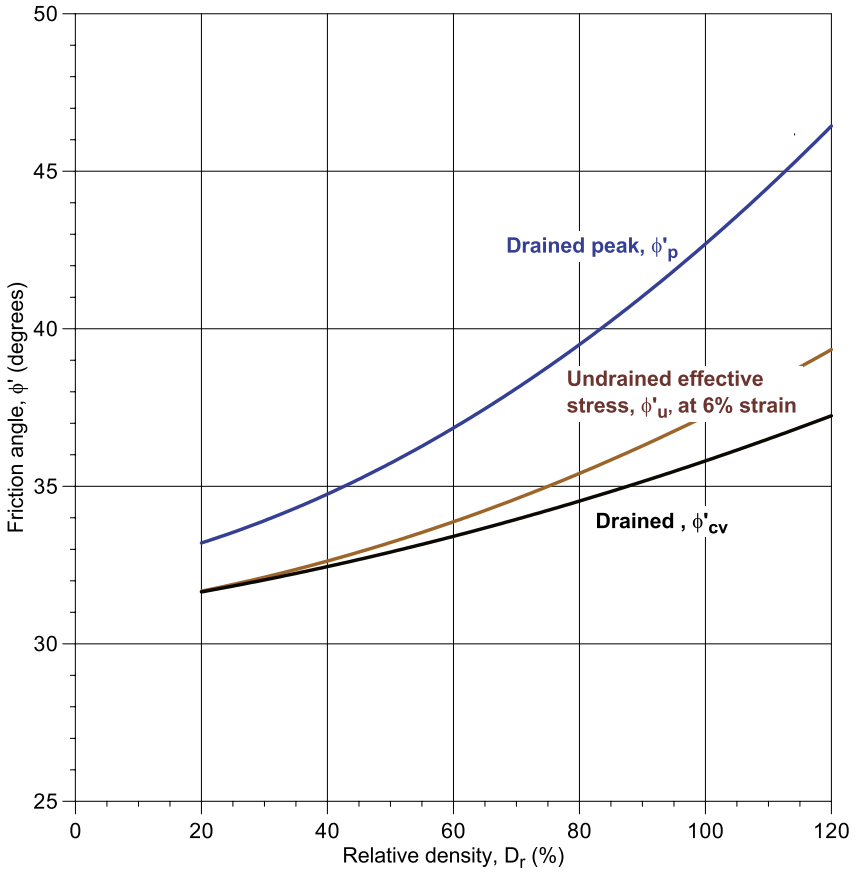

Fig. 6. Comparison of drained peak, constant volume, and undrained effective stress friction angles for the consolidation stress range of 250–500 kPa

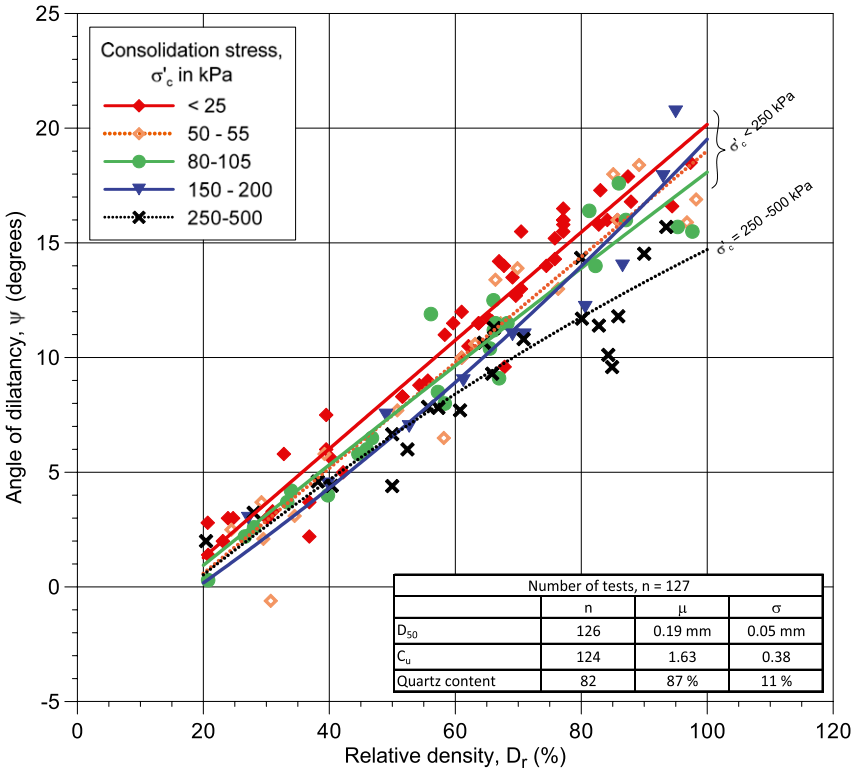

Fig. 7. (Color) Tangent dilatancy angle at peak shear stress as a function of D_r and σ'_c

J. Geotech. Geoenviron. Eng., 2013, 139(7): 1140-1155

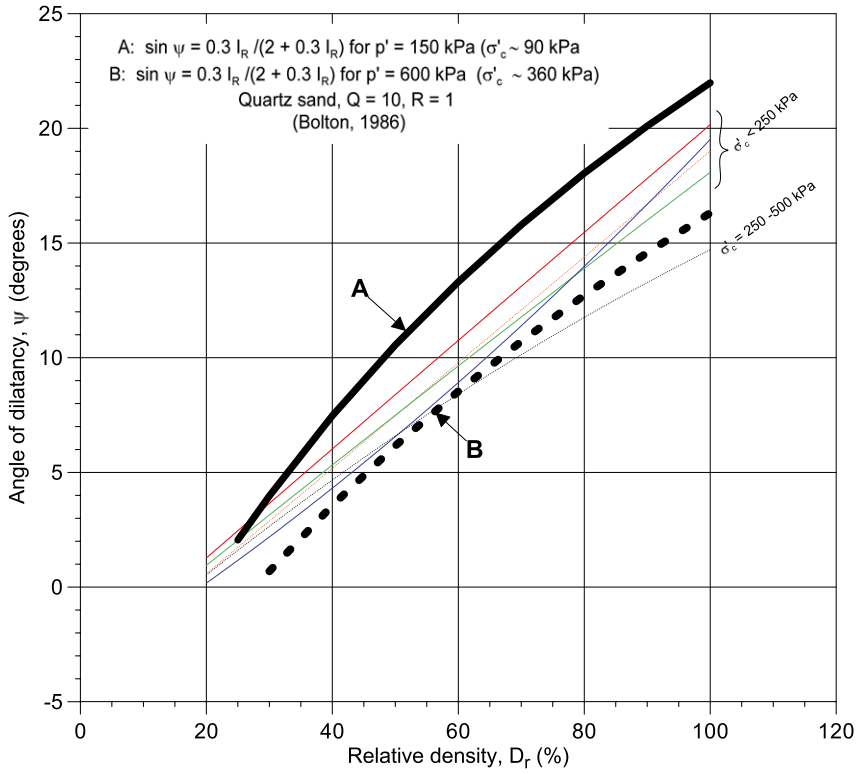

Fig. 8. Tangent dilatancy angle at peak shear stress compared with Bolton (1986)

previous maximum stress. By visual inspection of the example in Fig. 10 it can be seen that the proposed formulas are able to give excellent agreement with the measured behavior. The formulas capture the differences in moduli for virgin loading, unloading, and reloading, as well as the nonlinearity within each of these loading branches.

The best-fit parameters are given in Table 1. The constrained modulus will depend on several factors, such as the grain size, density, water content, angularity, and mineralogy. The best-fit m and n parameters for all the tests in the database were attempted correlated with the index parameters, such as the water content, void ratio, and grain size. However, the database was not extensive enough to establish correlations with all factors that influence the behavior. Because the effect of all the factors could not be singled out, there will also be scatter and uncertainty in the correlations that were established.

The parameters m and n are not independent, and the parameter set that gave the best overall fit was used. The best-fit curves that are drawn in Figs. 11–14 are based on visual judgment. The correlations are presented in Figs. 11–15. The labels give the data for each individual test, and the curves are estimated average values. The plots are for the noncalcareous soils.

Correlations for Virgin Modulus Number m_l and Virgin Modulus Exponent n_l

In Fig. 11, the virgin loading modulus number, m_l, is plotted as a function of D_{10} with water content as the parameter. The virgin modulus number increases with decreasing initial water content and increasing grain size. In Fig. 12, the virgin loading modulus exponent, n_l, is plotted as a function of the grain size parameter D_{10} with water content as the parameter. There is scatter in the virgin modulus exponents with no obvious trend with respect to water content or grain size; however, a constant value of $n_l = 0.65$ is proposed for $D_{10} < 0.15$ mm, with a reduction in n_l for $D_{10} > 0.15$ mm.

Correlation for Unloading Modulus Number m_u and Exponent n_u

The modulus expression contains many parameters that depend on each other. To facilitate the correlations, the best fit for unloading was made by assuming a constant unloading exponent, n_u, and to correlate the unloading modulus number, m_u, with the virgin modulus number, m_l. Based on some initial attempts, it was decided to assume an unloading exponent of $n_u = 1.05$. In Fig. 13, the ratio between the virgin loading and unloading modulus numbers, m_l/m_u, is plotted as function of m_l with water content as the parameter. The ratio between the modulus numbers, m_l/m_u, increases with increasing virgin modulus number, m_l, with no obvious trend with respect to water content or void ratio. It is proposed to determine m_u from the correlations given in Fig. 13, which can also be written as

$$m_u = 8, \quad \text{when } m_l \le 200$$
$$m_u = m_l/[25 + 0.28 \cdot (m_l - 200)], \quad \text{when } m_l > 200$$

Correlations for Reloading Modulus Number m_r and Exponent n_r

As for unloading, the best fit for reloading was made by assuming a constant exponent and correlating the modulus number with the

J. Geotech. Geoenviron. Eng., 2013, 139(7): 1140-1155

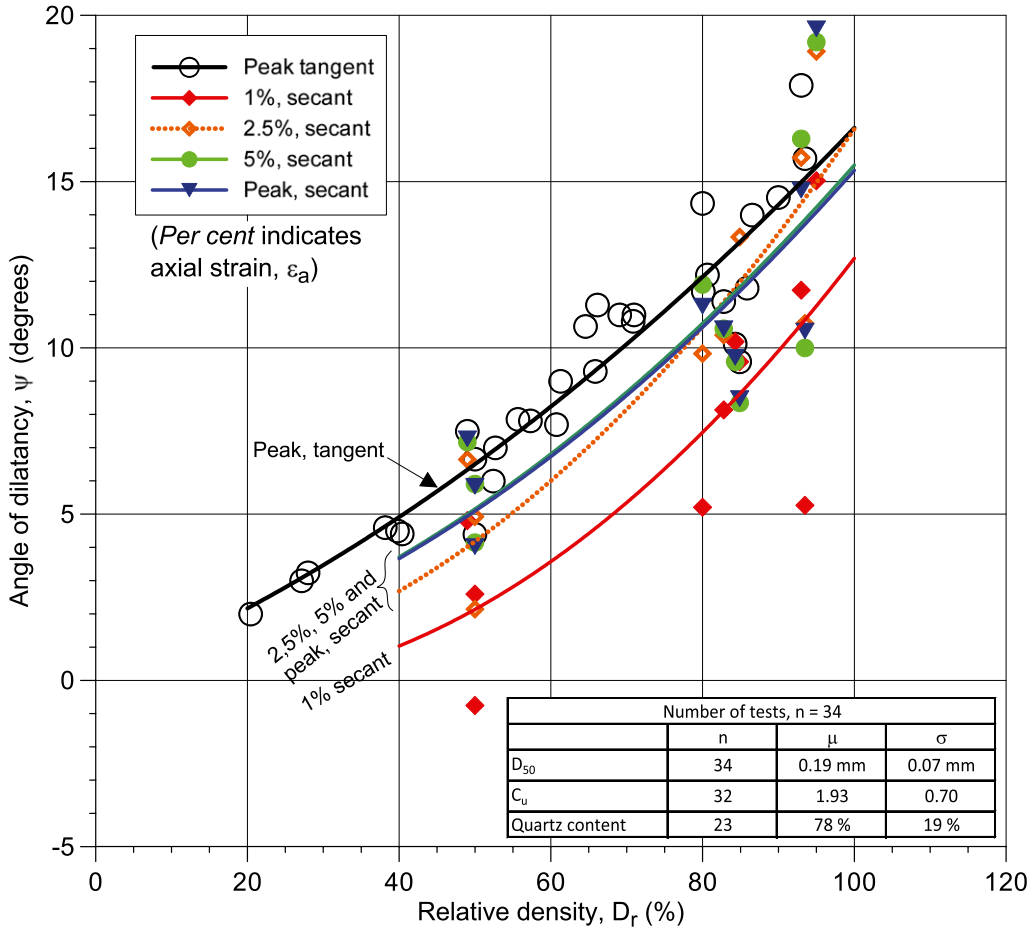

Fig. 9. (Color) Secant dilatancy angle at various strains and tangent dilatancy angles at peak shear stress as a function of D_r for $\sigma_c' = 150 - 450$ kPa

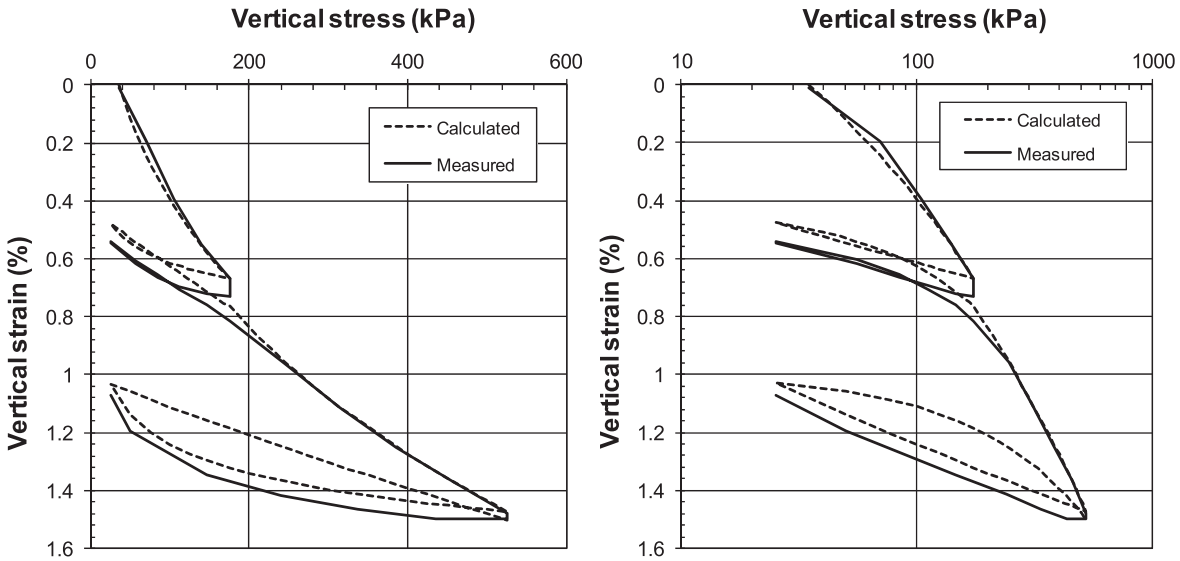

Fig. 10. Examples of measured and calculated vertical strains with best-fit parameters

Table 1. Index Properties and Best-Fit Parameters for the Oedometer Test in Fig. 10

	Grain size (mm)				Loading		Unloading		Reloading	
Water content (%)	< 0.002 (%)	< 0.06 (%)	D_{10}	D_{60}	m_l	n_l	m_u	n_u	m_r	n_r
27.5	0	60	0.018	0.073	225	0.67	5.7	1.05	1.7	0.1

J. Geotech. Geoenviron. Eng., 2013, 139(7): 1140-1155

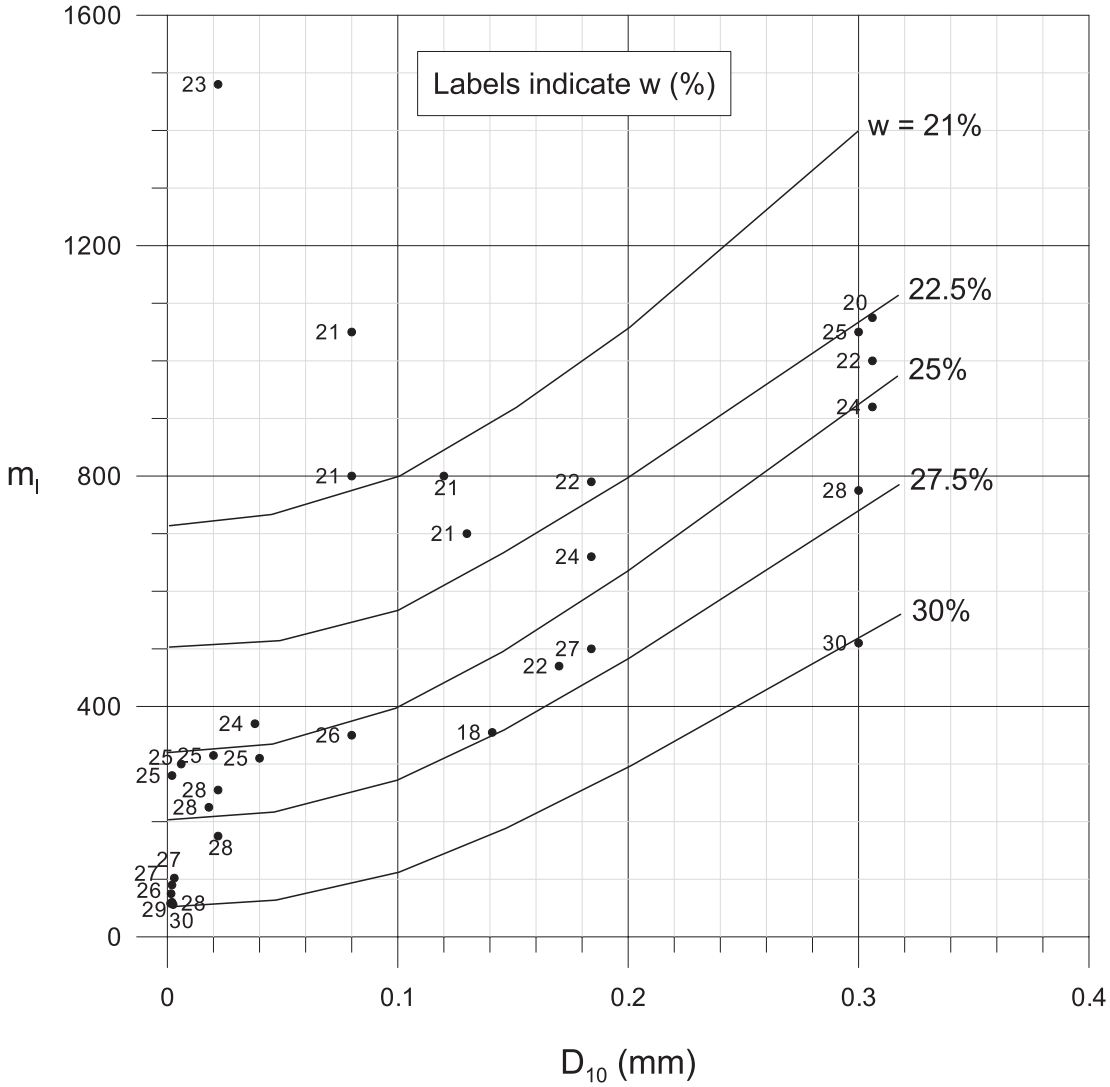

Fig. 11. Modulus number for virgin loading, m_l, as a function of D_{10} (best fit for individual tests and curves for the overall average)

virgin modulus number, m_l. Based on some initial attempts, it was found justified to assume a reloading exponent of $n_r = 0.1$. In Fig. 14, the ratio between the virgin loading and reloading modulus numbers, m_l/m_r, is plotted as function of m_l with water content as the parameter. The ratio between the modulus numbers, m_l/m_r, increases with increasing virgin modulus number, m_l, with no obvious trend with respect to water content or grain size. It is proposed to determine m_r from the correlations given in Fig. 14, which can also be written as

$$m_r = 3.3, \quad \text{when } m_l \leq 200$$

$$m_r = m_l/[60 + 0.6 \cdot (m_l - 200)], \quad \text{when } m_l > 200$$

The ratio between the unloading and reloading modulus numbers, m_u/m_r, is plotted as function of the virgin loading modulus number, m_l, in Fig. 15. The ratio is given for the individual tests, and the curve shows the relationship based on the proposed equations in Figs. 13 and 14. The plot in Fig. 15 shows that there is considerable scatter in the m_u/m_r ratio, and that there can be significant deviations from the proposed relationship. There is no obvious correlation with the initial water content.

Discussion of Constrained Modulus Parameters

The proposed modulus number, m_l (Fig. 11) was tested by calculating the behavior of the individual tests from both the average curves in the diagrams and the best-fit parameters for each test. The comparison is summarized in Table 2, which shows the mean ratio between the calculated values of strains for virgin loading to $\sigma'_v = 200$ and 400 kPa. The comparison was made by calculating the mean value and SD (1) for all tests and (2) by excluding tests that gave a ratio outside a range of 0.5–2.

The proposed modulus numbers and exponents for unloading and reloading were tested by calculating the reloading modulus for the following two cases:

1. The secant reloading modulus when reloading from 100 to 200 kPa after first loading from 0 to 200 kPa and unloading to 100 kPa; and
2. The secant reloading modulus when reloading from 200 to 400 kPa after first loading from 0 to 400 kPa and unloading to 200 kPa.

The ratio between the values using the proposed curves and the values from the best-fit parameters for each test is presented in Table 2, which shows a high SD, indicating that the proposed parameter correlations should be used with care.

J. Geotech. Geoenviron. Eng., 2013, 139(7): 1140-1155

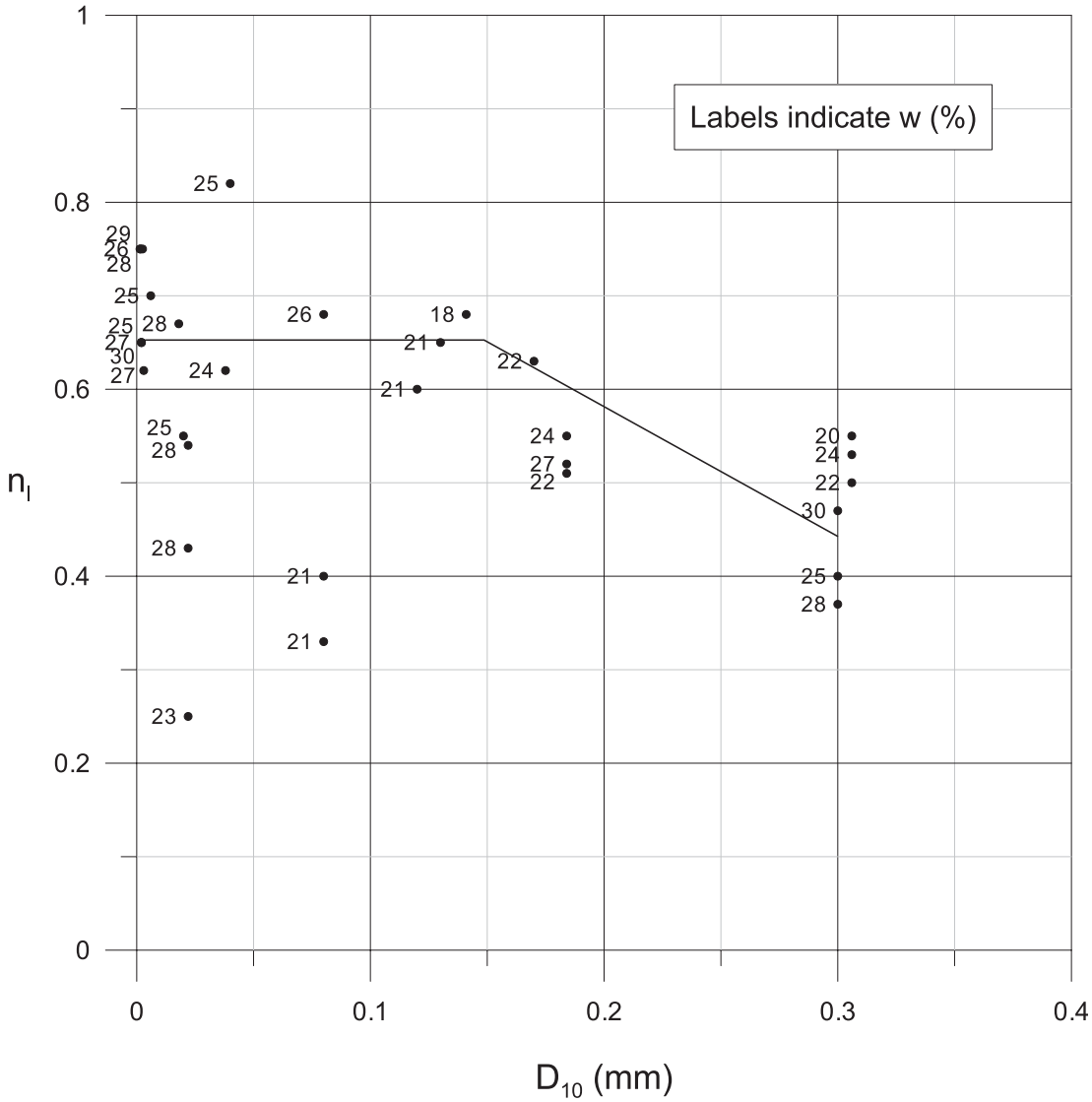

Fig. 12. Modulus exponent for virgin loading, n_l, as a function of D_{10} with initial water content as the parameter (best fit for individual tests and curves for the overall average)

Calcareous Soils

The database also contains data from oedometer tests on calcareous soils. However, the virgin loading modulus number for the calcareous soils were not included in Figs. 11–15 because m_l and n_l for calcareous soils had a significant scatter, and in some cases deviated significantly from the proposed curves. In some of the calcareous soils the best-fit n_l value was actually negative, meaning that the compressibility increases with increasing vertical effective stress. This is different from the noncalcareous soils, where the compressibility decreases with increasing vertical stress, as can be seen from the example in Fig. 10. The unloading modulus number, m_u, was significantly higher for calcareous than for noncalcareous soils; m_u can be a factor of 10 higher for calcareous than for noncalcareous soils. This may be explained by interlocking of the angular calcareous particles. However, the unloading modulus exponent did not seem to deviate significantly from the noncalcareous soils. None of the tests on calcareous soil in the database had reloading. However, it is expected that the reloading modulus number also would be higher than for noncalcareous soils.

Coefficient of Permeability (k)

The coefficient of permeability database contains permeability measurements from 63 triaxial and 96 oedometer tests on 34 different sands, silts, and clays. The permeability of saturated soils will depend on the particle size, void ratio, mineral composition, and fabric (e.g., Lambe and Whitman 1969). The clays in the database are marine clays with a wide range in plasticity from nonplastic to highly plastic with a plasticity index up to $I_p = 80 - 90\%$. The clay content ranges from very low to about 85%. The activity, which gives an indication of the mineral composition, is generally low to medium (activity $= I_p/\%$ clay $= 0.4 - 1.4$). The sands and silts are mainly quartz minerals with a range of angularity from subrounded to angular. According to Lambe and Whitman (1969), the mineral composition is of little importance with silts, sands, and gravels, apart from the content of mica and organic matter.

In the oedometer tests at NGI the coefficient of permeability was generally determined throughout the test by back-calculation from the measured pore-water pressure in constant rate of strain consolidation (CRSC) tests and from the time history of the various load

J. Geotech. Geoenviron. Eng., 2013, 139(7): 1140-1155

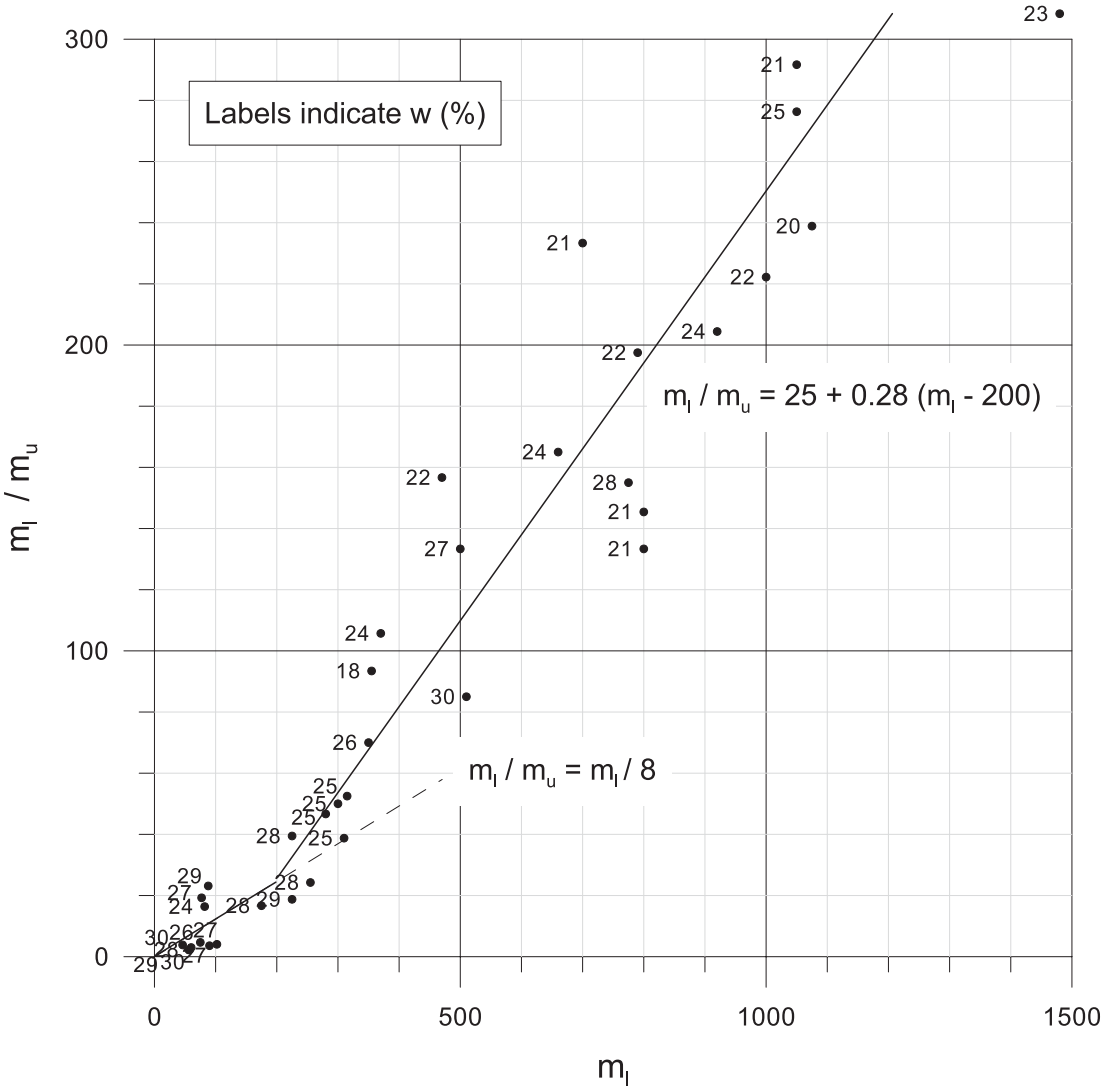

Fig. 13. Ratio between virgin loading and unloading modulus numbers, m_l/m_u, as a function of m_l with water content as the parameter, assuming $n_u = 1.05$ (best fit for individual tests and curves for the overall average)

increments in incremental loading (IL) tests. Flow measurements at two different stages of the test were, in most cases, also performed in both the CRSC and IL tests. The coefficient of permeability was extrapolated to the initial void ratio. In the triaxial tests, the permeability was generally measured only at the end of consolidation.

The specimens were prepared directly from intact samples or prepared by wet compaction, and the permeability properties corresponded to vertical flow. According to Terzaghi et al. (1996), the coefficient of permeability for flow in the horizontal direction will be about the same as in the vertical direction for homogeneous soft marine clays. However, in general the horizontal permeability can be higher than the vertical by a factor of 1.0–10, depending on factors such as the soil fabric anisotropy, varied nature of lacustrine deposits, and layering. All permeability values were measured on water-saturated samples at temperatures of about 20°C. The coefficient of permeability at 5°C will be about two-thirds of the coefficient of permeability at 20°C (e.g., Hazen 1920). The best correlation of the coefficient of permeability with the index parameters was found by plotting the coefficient of permeability as a function of the void ratio and clay content for soils with more than 10% clay content (Fig. 16), and as a function of D_{10} and the void ratio for soils with less than 10% clay content (Fig. 17). Figs. 16 and 17 also present the water content calculated based on the void ratio and the average unit weight of soil particles for the data set. The maximum difference in the unit weight of the soil particles in the data set gives an inaccuracy in the calculated water content of less than ± 3.5%. The proposed curves in Fig. 16 are supported by the variation in permeability measured during the CRSC tests. These results are not included because of space limitations.

The coefficient of permeability determined by the formula from Hazen (1920), $k = C_1 \cdot D_{10}^2$, with $C_1 = 100$ cm^{-1}s^{-1} and D_{10} (in cm), is included in Fig. 17. Hazen's formula with $C_1 = 100$ cm^{-1}s^{-1} seems to agree best for a void ratio of about $e = 0.7$ (water content of about $w = 26\%$) when the clay content is less than 10%. However, for a void ratio higher or lower than $e = 0.7$ the coefficient of permeability in the database can deviate significantly from Hazen's formula. Based on the data from Louden (1952), Terzaghi et al. (1996) stated that Hazen's formula may overestimate or underestimate the coefficient of permeability by a factor of 2. Carrier (2003) summarized recommendations with respect to Hazen's formula given in 10 different textbooks. Eight of these textbooks gave ranges of permeability within a factor of about 2 higher or lower. However, Lambe and Whitman (1969) reported permeabilities that were 1–42% of the Hazen's formula, and Mansur and Kaufman

J. Geotech. Geoenviron. Eng., 2013, 139(7): 1140-1155

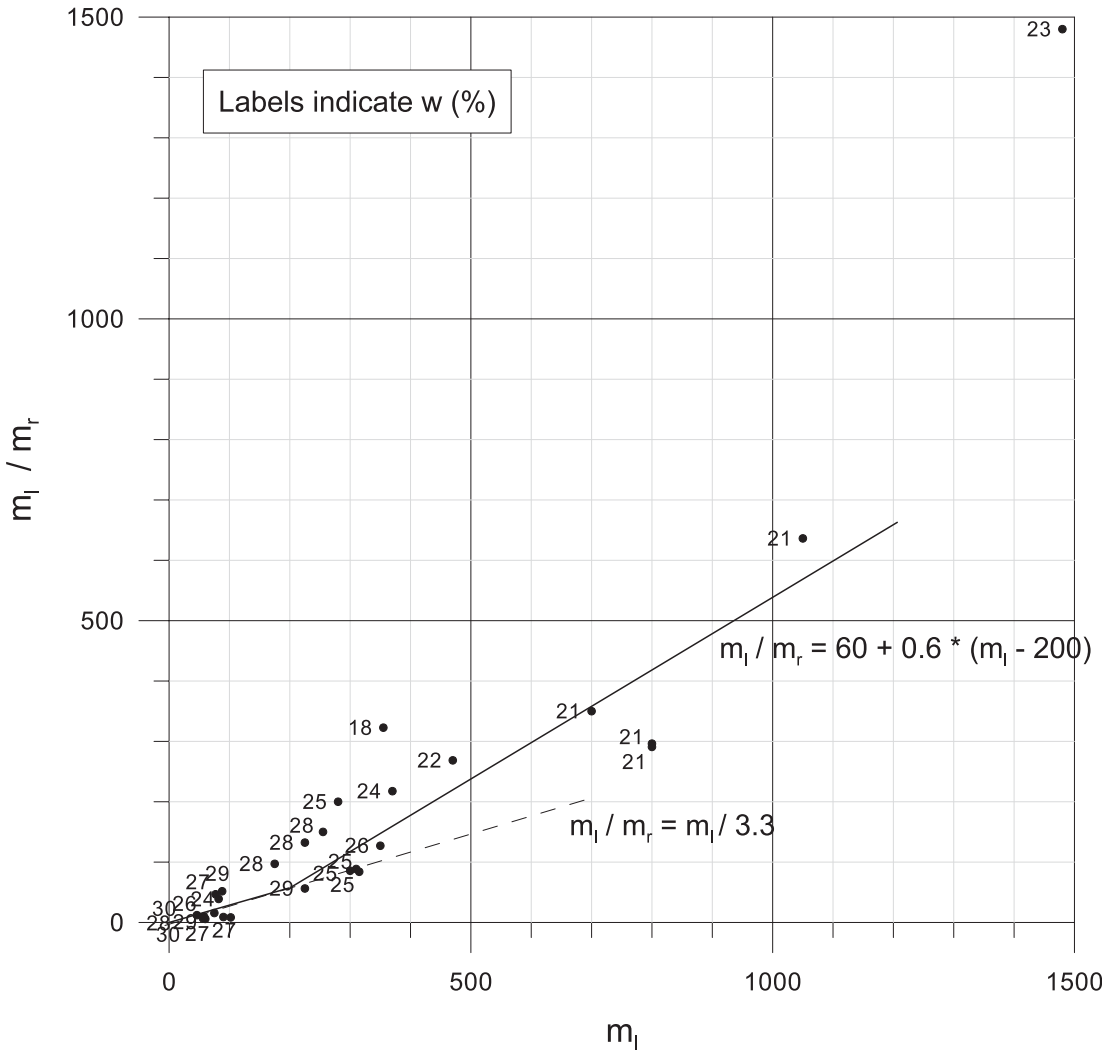

Fig. 14. Ratio between virgin loading and reloading modulus numbers, m_l/m_u, as a function of m_l with water content as the parameter, assuming $n_r = 0.1$ (best fit for individual tests and curves for the overall average)

(1962) reported permeabilities that were 1–10 times higher than Hazen's formula. The data in Fig. 17 indicate that the deviation can be much larger than a factor of 2, and that it may depend on the void ratio (or water content).

The data in Fig. 17 have a coefficient of uniformity within the range of $C_u = D_{60}/D_{10} = 1.5 - 4$ for the soils with less than 10% clay content. There was no detectable trend for the data to depend on C_u. This is in agreement with the laboratory studies on natural sands and gravels with subangular grains by Kenney et al. (1984), who found that the permeability was little influenced by C_u within the range of $C_u = 1.04 - 12$. However, Kjærnsli et al. (1992) reported data that were lower than Hazen's formula, and that the difference increased with increasing C_u.

It is recommended to use Fig. 16 when the clay content is more than 10% and Fig. 17 when the clay content is less than 10%, and to be cautious when using the diagrams for soils that are different from those in the database described previously.

Summary and Conclusions

The paper presents diagrams of the (1) drained and undrained friction angles of sand; (2) dilatancy angle of sand; (3) parameters in a nonlinear constrained modulus expression for virgin loading, unloading, and reloading on sand and silt; and (4) diagrams with the coefficient of permeability for sand, silt, and clay. The diagrams are compiled from data in the NGI files and published literature.

Friction Angles

The data show that the drained peak, constant volume, and undrained effective stress friction angles (ϕ'_p, ϕ'_{cv}, and ϕ'_u) all increase with increasing relative density, and that ϕ'_p is significantly higher than ϕ'_{cv} and ϕ'_u at high D_r. The difference is less at lower D_r; ϕ'_p and ϕ'_{cv} increase with decreasing consolidation stress, σ'_c, whereas ϕ'_u depends less on σ'_c.

Dilatancy Angle

The dilatancy angle, ψ, increases with increasing D_r; ψ increases with decreasing σ'_c at high D_r.

Constrained Modulus

The constrained moduli for virgin, unloading, and reloading are expressed by a nonlinear formulation. An attempt was made to establish correlations between the parameters in this formulation and

J. Geotech. Geoenviron. Eng., 2013, 139(7): 1140-1155

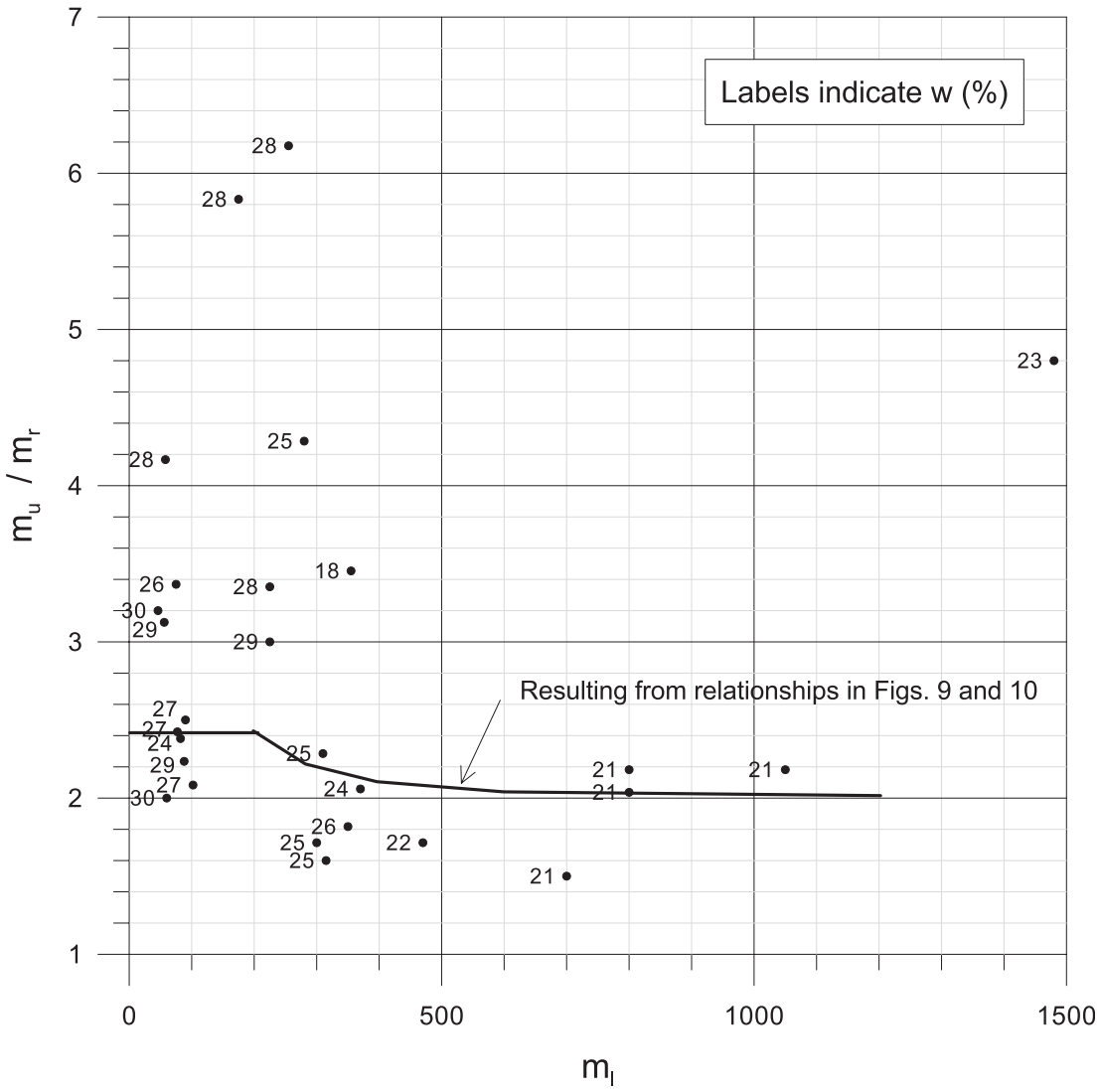

Fig. 15. Ratio between unloading and reloading modulus numbers, m_u/m_r, as a function of m_l (best fit for individual tests and curves for the overall average; initial water content as the parameter)

Table 2. Mean Ratios for the Virgin Strain and Reloading Modulus

	Virgin strain ratio (σ'_v = 200/400 kPa)			Reloading modulus ratio (σ'_v = 100 to 200/200 to 400 kPa)		
Data points	Average	SD	Number of tests	Average	SD	Number of tests
All	0.91/0.88	0.42/0.36	36	1.67/1.72	1.53/1.57	27
Excluding tests with ratios outside 2 and 0.5	1.03/0.99	0.35/0.27	30	1.11/1.10	0.49/0.47	19

Note: Ratios calculated as the value with parameters from the average curves in Fig. 11 divided by the value from the best-fit parameters (noncalcareous soils).

index parameters such as water content, void ratio, and grain size parameters. Correlations based on water content and D_{10} are proposed for noncalcareous soils. However, the constrained modulus also depends on other factors, like angularity and mineralogy, and the correlations have high standards of deviation. Therefore, the correlations should only be used for rough estimates, and design should be based on site-specific tests.

The oedometer data show that significant creep can occur in silt and sand. Creep was not included in the proposed constrained modulus expressions, which refer to the modulus from the constant rate of strain tests or incremental loading tests with short duration load increments. For calcareous soils, the constrained modulus shows significant scatter and can deviate significantly from the behavior predicted by the parameters proposed for noncalcareous soils.

Coefficient of Permeability

The proposed correlations present the coefficient of permeability as a function of D_{10} and water content for soils with less than 10% clay

J. Geotech. Geoenviron. Eng., 2013, 139(7): 1140-1155

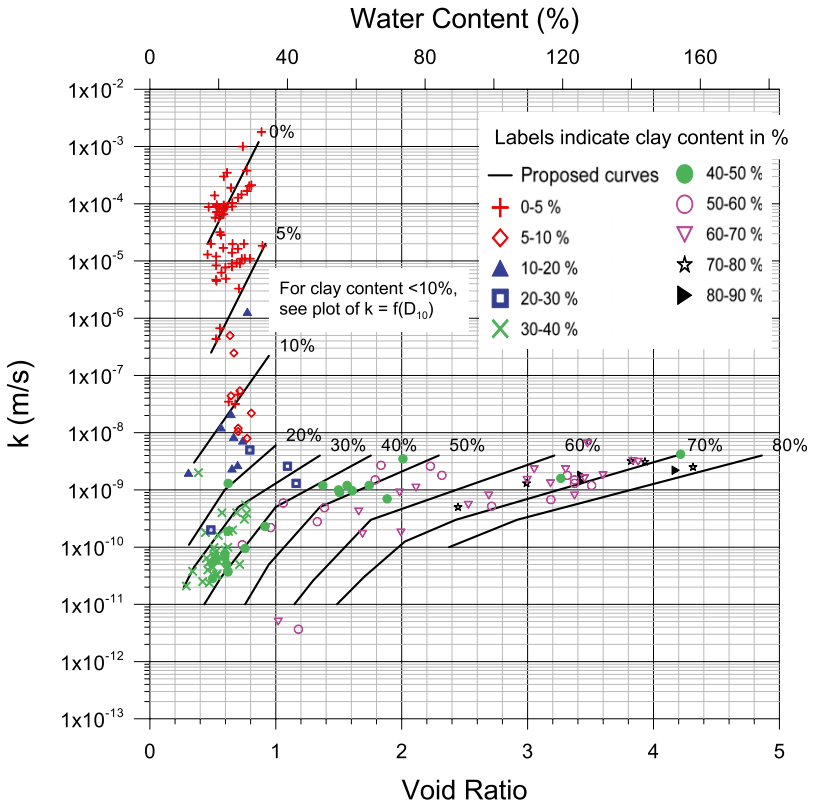

Fig. 16. (Color) Coefficient of permeability, k, as a function of the void ratio, water content, and clay content

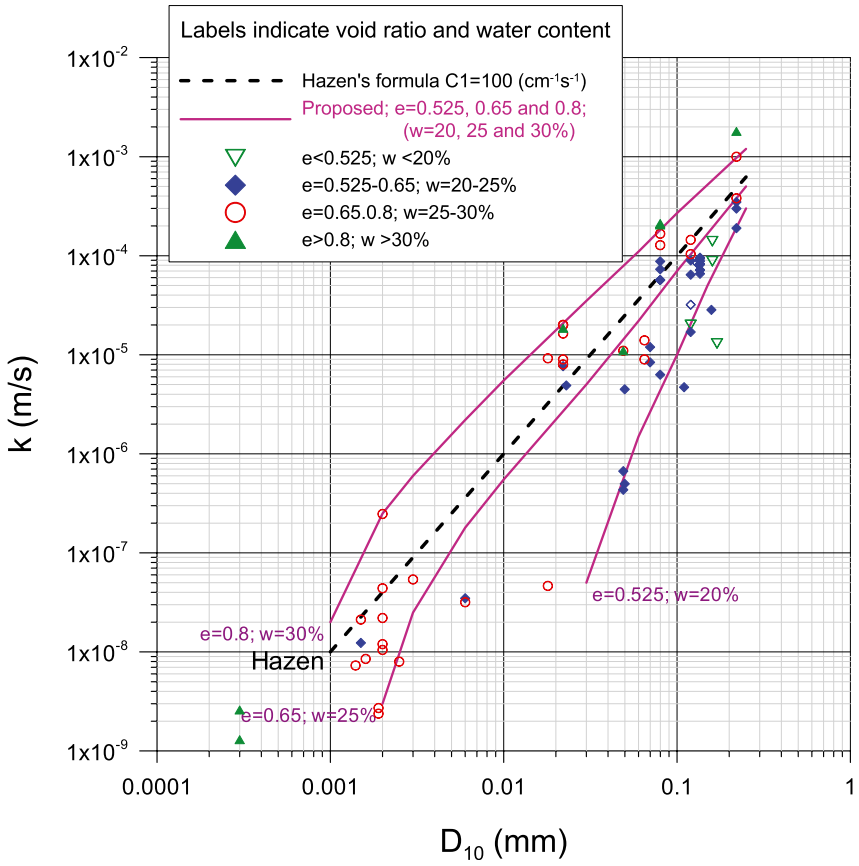

Fig. 17. (Color) Coefficient of permeability, k, as a function of D_{10}, void ratio, and water content

J. Geotech. Geoenviron. Eng., 2013, 139(7): 1140-1155

content and as a function of water content and clay content for soils with more than 10% clay content. Hazen's formula agrees best with the data for soils with less than 10% clay content and a water content of 26%; however, it can deviate significantly for higher and lower water content.

Acknowledgments

The work to establish the diagrams in this paper is funded by the Research Council of Norway. The data used are based on information from research projects sponsored by the Research Council of Norway, joint industry sponsored projects, and consulting projects. Dr. Hans Petter Jostad and numerous other NGI colleagues have contributed to the results. This cooperation is greatly appreciated.

References

Andersen, K. H. (2009). "Bearing capacity under cyclic loading—Offshore, along the coast, and on land. The 21st Bjerrum Lecture presented in Oslo, 23 November 2007." *Can. Geotech. J.*, 46(5), 513–535.

Andersen, K. H., Lunne, T., Kvalstad, T. J., and Forsberg, C. F. (2008). "Deep water geotechnical engineering." *Proc., XXIV Mexican Society Conf. on Soil Mechanics*, Vol. IV, Sociedad Mexicana de Mecánica de Suelos, Mexico City.

Bjerrum, L. (1973). "Problems of soil mechanics and construction on soft clays and structurally unstable soils." *Proc., 8th Int. Conf. on Soil Mechanics and Foundation Engineering*, Vol. 3, 111–159, USSR National Society for Soil Mechanics and Foundation Engineering, Moscow.

Bolton, M. D. (1986). "The shear strength and dilatancy of sands." *Geotechnique*, 36(1), 65–78.

British Standards Institute (BSI). (1990). "Methods of tests for soils for civil engineering purposes." *BS 1377*, London.

Carrier, D. W. (2003). "Goodbye, Hazen; hello, Kozeny-Carman." *J. Geotech. Geoenviron. Eng.*, 129(11), 1054–1056.

Hardin, B. O., and Drnevich, V. P. (1972). "Shear modulus and damping in soils: Design equations and curves." *J. Soil Mech. and Found. Div.*, 98(7), 653–665.

Hazen, A. (1920). "Hydraulic-fill dams." *Trans. Am. Soc. Civ. Eng.*, 83(1), 1713–1745.

Janbu, N. (1963). "Soil compressibility as determined by oedometer and triaxial tests." *Proc., European Conf. on Soil Mechanics and Foundation Engineering*, Vol. I, Deutsche Gesellschaft für Erd- und Grundbau e.V, Essen, Germany.

Kenney, T., Lau, D., and Ofoegbu, G. I. (1984). "Permeability of compacted granular material." *Can. Geotech. J.*, 21(4), 726–729.

Kjærnsli, B., Valstad, T., and Hoeg, K. (1992). *Rockfill dams. Design and constructions*, Tapir, Trondheim, Norway.

Ladd, C. C., Foot, R., Ishihara, K., Schlosser, F., and Poulos, H. G. (1977). "Stress deformation and strength characteristics." *Proc., 9th Int. Conf. on Soil Mechanics and Foundation Engineering*, Vol. 2, 421–494, Japanese Society of Soil Mechanics and Foundation Engineering, Tokyo.

Lambe, T. W., and Whitman, R. V. (1969). *Soils mechanics*, Wiley, New York.

Louden, A. G. (1952). "The computation of permeability from simple soil tests." *Geotechnique*, 3(4), 165–183.

Lunne, T., and Andersen, K. H. (2007). "Soft clay shear strength parameters for deepwater geotechnical design." *Proc., 6th Int. Offshore Site Investigation and Geotechnics Conf. on Confronting New Challenges and Sharing Knowledge*, 151–176. Society for Underwater Technology, London.

Mansur, C. I., and Kaufman, R. I. (1962). "Dewatering." *Foundation engineering*, G. A. Leonards, ed., McGraw Hill, New York, 241–350.

Schmertmann, J. H. (1978). "Guidelines for cone penetration tests. Performance and Design." *FHWA-TS-78-209*, U.S. Dept. of Transportation, Federal Highway Administration, Washington, DC.

Terzaghi, K., Peck, R. B., and Mesri, G. (1996). *Soil mechanics in engineering practice*, 3rd Ed., Wiley, New York.